

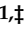
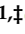







Article

A Quasi-Wireless Intraoperative Neurophysiological Monitoring System

Eduardo Alonso Rivas ^{1,†,‡}, Romano Giannetti ^{1,‡}, Carlos Rodríguez-Morcillo García ^{1,‡},
Javier Matanza Domingo ^{1,‡}, José Daniel Muñoz Frías ^{1,‡}, Graziella Scandurra ^{2,*,‡}, Carmine Ciofi ^{2,‡},
Lorena Vega-Zelaya ^{3,‡} and Jesús Pastor ^{3,‡}

¹ Instituto de Investigación Tecnológica, Universidad Pontificia Comillas, 28015 Madrid, Spain

² Dipartimento di Ingegneria, Università degli Studi di Messina, 98166 Messina, Italy

³ Clinical Neurophysiology and Instituto de Investigación Biomédica, Hospital Universitario La Princesa, 28006 Madrid, Spain

* Correspondence: gscandurra@unime.it

† Current address: Soinde s.l., Calle Burdeos 12B, Las Rozas de Madrid, 28232 Madrid, Spain.

‡ These authors contributed equally to this work.

Abstract: Intraoperative Neurophysiological Monitoring is a set of monitoring techniques that reads electrical activity generated by the nervous system structures during surgeries. In non-trivial surgeries, neurophysiologists require a significant number of electrical signals to be picked up to check the effects of the surgeon's actions in real time or to confirm that the correct nerves are selected. As a result, cabling the patient in the operating room can become cumbersome. The proposed WIONM module solves part of the problem by converting a good part of those cables into a wireless connection that is substantially transparent to the human operator and the existing medical instrumentation.

Keywords: intraoperative monitoring; ECG; EMG; EEG; MEP; SSEP; AEP; wireless



Citation: Alonso Rivas, E.; Giannetti, R.; Rodríguez-Morcillo García, C.; Matanza Domingo, J.; Muñoz Frías, J.D.; Scandurra, G.; Ciofi, C.; Vega-Zelaya, L.; Pastor, J.

A Quasi-Wireless Intraoperative Neurophysiological Monitoring System. *Electronics* **2022**, *11*, 3918. <https://doi.org/10.3390/electronics11233918>

Academic Editor: Enzo Pasquale Scilingo

Received: 28 October 2022

Accepted: 24 November 2022

Published: 27 November 2022

Publisher's Note: MDPI stays neutral with regard to jurisdictional claims in published maps and institutional affiliations.



Copyright: © 2022 by the authors. Licensee MDPI, Basel, Switzerland. This article is an open access article distributed under the terms and conditions of the Creative Commons Attribution (CC BY) license (<https://creativecommons.org/licenses/by/4.0/>).

1. Introduction

Intraoperative Neurophysiological Monitoring (IONM) [1] is a set of techniques that provide increased functional knowledge of the nervous system structures during a surgical operation. This denomination includes both stimulus-based techniques, such as evoked potentials (EP), that measure the response to a previous stimulation, as well as free running techniques, in which signals are acquired continuously without any stimulus, such as Electroencephalography (EEG), Electromyography (EMG) and Electrocochleography (ECoG).

These tools are routinely used by the surgeon and the assisting neurophysiologist to identify and prevent possible injuries during the medical procedure [2]. Several tens of signals are often needed for the average process; the burden of cabling and connections around the operating table is a common cause of uneasiness for the medical and technical staff. Figure 1 shows an example of this situation. The picture was taken during the preparation of a surgery. All the cabling remains below the sterile drapes with the connection adapters below or hanging from the operating table, making it uneasy not only the preparation, but the access to the cables during the surgery in case it is needed. Eliminating or at least reducing the cabling complexity is seen as a big step towards a more efficient clinical practice during intraoperative monitoring. Reducing this cabling using a wireless system is the main objective of the work presented here.

The characteristics of the signals to be measured are also wildly different, running from relatively low-band and high-level ones (like ECG) to very low-level and relatively high-band ones, like EMG or EP. The analog front-ends must be configurable to pick and amplify all those kind of signals. The back-end systems used for the IONM are quite complex, too, running complex software which is often highly expensive and proprietary;

the medical staff is familiar with these systems and substituting them on a short or medium time scale is not really feasible for most medical centers.



Figure 1. Example of cabling during a surgery preparation with IONM. Note the bundle of coloured cables (electrodes) and the number of adapters of the monitoring system.

The designed system presented here is capable of substituting most of the cabling with a wireless system in an almost completely transparent way; the existing electrodes, electrode connectors, and integrated instrumentation can be used without major changes in the medical procedure (the only exception is the contact impedance evaluation procedure, as will be explained later). This focus makes the system quite different from other wireless physiological monitoring systems oriented to brain-computer interfaces ([3,4]), long term monitoring ([5–7]), or completely independent systems ([8,9]).

In brief, the system described here is intended to sense and register analog biological neurophysiological signals coming from neural activity, transmit and reproduce them with the same analog characteristics. Input of the system will be the sensing electrodes connected to the patient, whereas the output will be connected to a conventional IOM system. Additionally, the system must adapt automatically and transparently to the amplitude range of the signal sensed on each channel.

Moreover, the system presents a minimal user interface with two purposes: on the one hand, a set of switches is utilized to configure each channel in referential (single-ended) or differential mode, as well as change the input reference between ground or any other channel. An additional switch permits selecting between normal acquisition mode or impedance measurement mode, needed to insure that excessive contact impedance does not compromise the signal quality [10–12]. Incorrect value of contact resistance and configuration status of the analog front-end is indicated visually by means of an array of multicolor LEDs.

In broad terms, as depicted in Figure 2, the system can be divided in Transmitter, communication link (also referred to as RF link) and Receiver. Each of these system components will be discussed in the following sections.

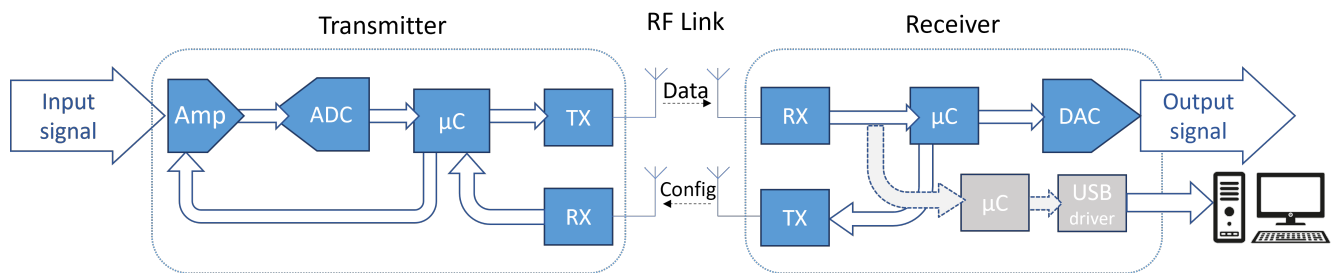


Figure 2. Schematic of the system. The input signal is delivered through standard surface or needle electrodes; the output system is normally the existing IONM setup of the medical facility.

In Section 2 the theoretical framework for the system is summarized. In Section 3, the hardware of the system is described, with subsection dedicated to explain the design of the transmitter, receiver and the debugging/tracking system used during verification. Next, in Section 4, the experimental results are reported, both from laboratory tests with reconstructed signals and in the field with human volunteers; finally, in Section 5, we discuss the measurements obtained and the effectiveness of the system.

2. Theoretical Framework

The fundamental idea of the system is to sample the input signals, transmit them in digital form, and then re-build the original signal at the end point, as shown in Figure 3. The measured signal is band-limited by the antialiasing filter, which removes all the signal components above band B (which in the presented system has been chosen to be 5 kHz). After the digitalization by the analog-to-digital converter (ADC), the signal is transmitted to the receiver. In the receiver device, it is transformed again into an analog signal by a digital-to-analog converter (DAC) and an anti-imaging filter. It is well known that when using the correct sample rate, antialiasing filter, and anti-imaging (reconstruction) filter, in absence of noise, and with a perfect analog to digital conversion, the output signal is guaranteed by the Shannon theorem [13] to be the same in band B .

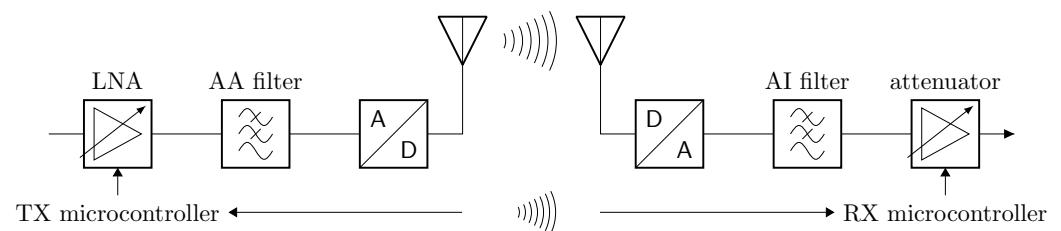


Figure 3. Theoretical operation of the system. The Low Noise Amplifier (LNA) and the programmable attenuator are coordinated by the two microcontrollers (in the transmitter and in the receiver) that cooperate to reconstruct the measured signal. The blocks in the figure represent, from left to right, the LNA, the anti-aliasing filter, the analog-to-digital converter, the digital-to-analog converter, the anti-imaging filter, and the programmable attenuator.

In the presence of noise, and due to the limited resolution of the ADC and DAC converters, there is a limit to the accuracy with which the input signal can be reproduced at the output; for this reason it is paramount to add the variable amplification and attenuation circuits, so that the full range of the ADC system is used all the time. In the proposed system, the adjustment of the two stages is made on-the-fly and in a transparent way, without the need for any intervention by the operator.

With the aforementioned conditions, the link is practically invisible to the instrumentation connected at its output, which acts as if the signal is arriving directly from the electrodes. The only exception is when there is the need to check the electrodes' connection impedance; this is resolved by performing that task in the transmitter and informing the operator of the results, as will be explained later.

3. WIONM Prototype

The prototype, called WIONM (Wireless IONM) from now on, is composed by a Transmitter, which is a compact module of about $15\text{ cm} \times 10\text{ cm} \times 2\text{ cm}$ (Figure 4, right), battery-powered, thought to be positioned near the site where the signals are connected—for example, fastened to the operating table head; and a line-powered Receiver (left), whose size is less important, located near the analyzing instrumentation. The receiver has no wires connected to the patient, so its positioning is easy and it can be located outside of the operation table.



Figure 4. Photo of the complete prototype; **left** side, the receiver, which will rebuild the original signals; **right** side, the transmitter, to which the electrodes will be connected.

3.1. Transmitter

Biological signals are sensed with the help of electrodes (surface or needle-ended) that are connected to the acquisition system through standard medical-safe DIN connectors (touch-proof). The prototype here described uses said connectors, followed by a differential amplifier with its corresponding filtering and conditioning circuitry. Due to the nature of the biological signals of interest, that range from μV to mV , and with wildly different bandwidth requirements [14], this is the most delicate and important part of the system. Accordingly, very high amplification and noise rejection is required. An in-house design based around very low noise instrumentation amplifiers (AD8429 [15]), digitally-controlled variable-gain amplifiers, passive contact impedance assessment, and aggressive anti-aliasing and high-pass filtering has been adopted [16–19], with a bandwidth ranging from 0.1 Hz to 5 kHz. In parallel to the acquisition hardware, as part of any of the commercial systems of this kind, an impedance measurement system is present in the analog part of the designed hardware. A detailed description of this section can be found in [16]. Although it is out of the scope of this paper, the noise of the analog front-end of the Transmitter was analyzed. Figure 5 shows the minimum noise obtained for the minimum possible input impedance.

Scalp measurements, useful for EEG and evoked potentials such as somato-sensory (SSEP) and auditory (AEP), as well as for brain-computer interfaces [20], are commonly registered referentially. This means that the input channels are acquired in single-ended fashion, and all the channels registered are referenced to the same electrode (whose positioning depend on the specific measurement required). On the other hand, muscle responses (EMG or motor evoked potentials (MEP)) are registered in differential mode, with a pair of electrodes per channel, plus a reference ground. Although the system is designed mainly

for differential inputs, a set of switches in the input are arranged in order to modify the input reference. This permits varying between single-ended and fully differential acquisition, providing high flexibility for any kind of signals. We opted for a modular system with a base unit hosting 8 differential channels in order to match industry standard.

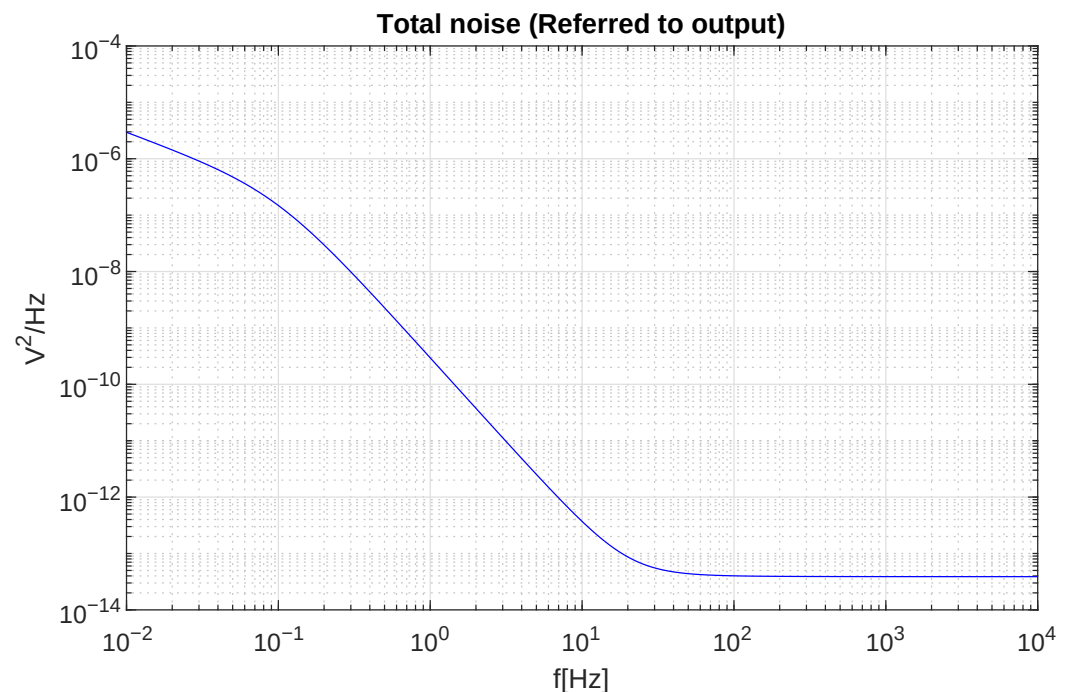


Figure 5. Minimum noise obtained for the analog front-end of the Transmitter device, measured at the output of the amplifier, with gain set to 50 V/V. The flat noise level corresponds to the expected input-referred noise for the AD8429, which is stated at around $3 \text{ nV}/\sqrt{\text{Hz}}$ [15].

Since signals of different amplitude ranges are to be utilized, it is important to have a set of variable gain amplifiers available. Commonly, the amplification gain is set by software by means of the user interface of the IOM system, but in this case the system modifies it automatically, through an amplitude evaluation algorithm that detects the voltage span of the signal. The dynamic range of the analog input design spans from $\pm 180 \mu\text{V}$ to $\pm 36 \text{ mV}$, depending on the variable gain selected for each channel. The analog signal is then sampled and digitized by means of a dedicated multichannel Analog to Digital Converter (ADC). Digital information is passed through a microcontroller that is in charge of managing the rest of the components via SPI protocol. Timing and synchronization are of paramount importance in order to comply with specific sampling frequency. The maximum delay between the sampling and processing of the analog signal is $112 \mu\text{s}$. Nevertheless, the total delay between the acquisition of the signal and the reconstruction is mainly affected by the communication process between Transmitter and Receiver, as it will be shown below. There are four processes managed by the microcontroller: sampling, modifying programmable amplification, handling data packaging and transmission as well as attending the interrupt request from incoming communications.

Moreover, the transmission device relies on a rechargeable battery pack that provides for an uninterrupted operation lasting 8 h. Battery level is also monitored by the controller and an acoustic signal is sent out with an integrated beeper when it reaches a low-level threshold. This battery provides high flexibility for the system, increasing ergonomics and allowing for shorter electrode wires, which is one of the main objectives of the design we propose.

The design and development of this device has been carried out taking into account medical regulation and ISO 60601 requirements. For this reason, the applied part (the part that is in contact with human tissue) is physically isolated from powering part via

multichannel digital insulators located downstream the ADC conversion, and the front-end amplifier stage is insulated up to 5 kV from external voltages.

3.2. Receiver

As stated before, this system is intended to create a wireless bridge between the signal sensed from the patient and a conventional monitoring system (Figure 2). The receiver device is in charge of reproducing such signal. This part is composed of a transmitter/receiver module, a microcontroller, an 8-channels parallel Digital to Analog Converter (DAC) with suitable anti-imaging filtering and an analog variable gain stage that adjusts the signal voltage range. The output of the system is available via touchproof standard connectors. The receiver also hosts the user interface consisting in a series of switches to configure the analog front end, and a set of LEDs that provide visual information regarding the state of the system (for example, the result of the impedance measurement process).

In normal operation mode, the Receiver device is in a passive state, waiting for the reception of data frames from the Transmitter. When a transmission frame is received by the corresponding transceiver, an interrupt request is generated and the microcontroller starts the extraction of the information received. This frame is then parsed and decoded and the data, channel per channel, is sent to the multichannel DAC modules, where analog signals are regenerated. Depending on the voltage range of the signal received, an analog gain selector modifies its amplitude.

The usual data flow goes from Transmitter to Receiver. This normal operation mode is abandoned when a configuration change is requested by the user via the user interface of the device. If one of the switches is activated, the Receiver device interrupts the reception of the frames and swaps to transmission state. Then, a configuration frame is sent from the receiver to the transmitter instructing the latter that a configuration change or an impedance measurement is requested. These changes are managed by a state machine programmed in the Receiver microcontroller so that data can be correctly interpreted. If a change in the input configuration is requested, the receiver will wait for a confirmation frame from the transmitter and if it is correct, a LED signal will indicate that the specific channel is configured in the requested mode. On the other hand, if an impedance measurement is started, a calculation period begins and all data is collected and analyzed and the result of the measurement is shown with a color coded LED visual flag, along with an acoustic signal indicating the end of the measurement. Further details on these methodology can be found in [16].

3.3. USB Tracker

Besides intermediate digital and analog signals debugging, the development process of the prototype required the implementation of a mechanism to assess the correctness of the information sent and received as part of the configuration protocol. To this end, and as shown in Figure 2, an additional microcontroller is added to the Receiver device in order to gather the messages exchanged between the master microcontroller and the receiving transceiver. This microcontroller essentially acts as a “sniffer”.

The information read is buffered, encapsulated and, taking advantage of the USB controllers and libraries available for the microcontroller, sent out to a PC via USB port. Micro-USB port and conditioning circuitry is arranged in the PCB of the prototype, permitting both programming of the micro-controllers and extracting the information. A common PC is utilized to get the data, acting as USB master.

With the help of open source software USBPcap, raw data from selected USB port is captured in a .pcap file. Matlab software is utilized to parse and check the information at bit level, verifying data integrity and consistency with data sent. Additionally, visual representation of the signals is carried out. It is worth mentioning that the system does not require the integration of an internal physical memory, since the sampling, processing, transmission, reception and reconstruction of the information is made in real time. Note that, if the the specifications on data format for the standard visualization system

were available, there would be no need to convert the received digital data into analog form. The sniffer could be used, in this case, to send digital acquired data directly to the visualization software.

3.4. Transmission Wireless Link

The main goal of the work we have done was to obtain a wireless system that enables the transmission of neurophysiological signals without the utilization of cables. To do so, several technologies were considered ([5,21,22]). Power consumption, simplicity, and especially latency (delay between recording and reconstruction of the signal) were the factors taken into account. Intra-operative monitoring involves analysing evoked potential responses with stimulus-response times in the order of milliseconds. Hence, communication protocols requiring data compression or buffering were discarded. Therefore, it was required the utilization of a technology with a bandwidth large enough to support the transmission of the registered data at the specific sampling frequency rate.

All these aspects led to the implementation of an ad-hoc radio-frequency communication link. A Nordic Semiconductor nRF24L01 transceiver chip and the corresponding conditioning circuit is utilized. This component permits the operation on the industrial, scientific and medical (ISM) band with a bandwidth of 2.4 GHz to 2.5 GHz. This component is SPI-controlled, as are all the other complex devices in the system. The peculiarity of the application oriented the choice toward a custom protocol instead of adopting a standard one (such as, for example, Bluetooth or WiFi).

Although, as discussed above, the usual data flow goes from Transmitter to Receiver, configuration commands need to be transmitted in the opposite direction. Since the Transmitter is intended to be close to the patient and the access to it will be limited due to ergonomic reasons during surgical procedures, the configuration control panel is located in the Receiver, which is out of the operating table and accessible to the staff. The control panel contains configuration switches as well as tri-color LEDs to inform the user about the configuration state. When the position of at least one of the switches of the control panel is modified, a configuration frame is sent from the Receiver to the Transmitter. The RF transceiver selected permits power down, standby, reception (RX) and transmission (TX) modes (not simultaneously). Time division duplexing was considered in the design process, but a settling time of 130 μ s for each mode switching made it unfeasible due to the bandwidth and transmission speed required for the application time constraints. Because of that, a second radio link is added, with one additional transceiver added to each device (Receiver and Transmitter), thus obtaining separate and independent channels for data and command exchange. Taking advantage of the flexibility of the transceivers, each link is configured to occupy a different band and use a different address.

3.4.1. Data Transmission

Digital data is encapsulated in a dedicated frame that consists, broadly speaking, in an identification header, timestamp and for each channel, digital data information (without compression) and a code indicating the gain utilized for the amplification of the sample sent. This frame is buffered in the transceiver of the Transmitter device byte per byte via SPI, alternating with sample extraction. The RF transceiver is configured to add two CRC bytes in order to add robustness to the transmission. Calculations were carried out to ensure that the combination of frame size, number of channels, bit resolution and sampling rate do not overpass maximum bandwidth of the transceiver (2 Mbps), according to (1).

$$\begin{aligned}
 \text{BitRate} = & ((\text{Data bits/measurement} + \text{Scale bits/measurement}) \cdot 8 \text{ channels} \\
 & + \text{address bytes} + \text{CRC bytes}) \cdot \text{sampling rate} \\
 = & ((16 \text{ bits/measurement} + 8 \text{ bits/measurement}) \cdot 8 \text{ channels} \\
 & + 4 \text{ bytes} + 2 \text{ bytes}) \cdot 8.93 \text{ kHz} = 1.923 \text{ Mbps.}
 \end{aligned} \tag{1}$$

The 8 channels do indeed fill the available bandwidth of the link. However, several 8-channel modules can be used at the same time. Clearly, each pair is going to employ different channels (two channels for each pair of devices); the specific radio devices used allow for up to a theoretical maximum of 30 pairs to be deployed, covering up to 240 channels without need to change the hardware.

The timestamp and identification header of the frames received are analyzed. If the samples are received in a sequential order, the communication link is considered to be stable. On the other hand, if some frames are missing, the link is considered below optimum or inadequate, depending on the number of samples lost. This verification is carried out continuously, and the status of the connection is shown through a LED in the control panel that can be activated in green, yellow or red, based on the degree of reliability of the link, so that the user can move or rearrange the devices of the system to provide a better line of sight between radios. Additionally, the system implements a safety feature that prevents that loss of several consecutive samples results in a blank or flat response in the output.

Because of the application for which our design is intended, the latency between recording and regeneration of the signal at the output of the Receiver has to be as short as possible. Nevertheless, an unavoidable delay has to be expected, due to the several processes involved in the data chain: sampling, digitizing, data buffering, SPI transmission to sending transceiver, data transmission, buffering at the receiver, data extraction via SPI, parsing and, finally, DAC conversion to reconstruct the analog signals. The time delay introduced by a few of these processes can be known and predicted because of the sequence programmed in the microcontroller, and is basically constant if the error rate of the RF link is low. In other cases, and especially as far as the time elapsed between transmission and reception of each single frame is concerned, there is a degree of uncertainty. In order to estimate the maximum delay in a worst case scenario, systematic measurements are performed under laboratory conditions monitoring the activity of the SPI buses in the Receiver and the Transmitted during data exchange.

Figure 6 shows logic-analyzer measurements of SPI bus activity in the Transmitter (TX) and in the Receiver (RX) during data exchange. The portion of the data highlighted by the left-most blue square corresponds to the insertion of a known sequence of data in the transmitting buffer of the radio, while the portion of the data highlighted by the blue square at close to the bottom/right end of the figure in the right corresponds to the extraction of said data from the receiver radio FIFO. As the time marker shows, the delay between transmission and reception is lower than 500 μ s, acceptable for the required performance, as it will be discussed later on in the paper.

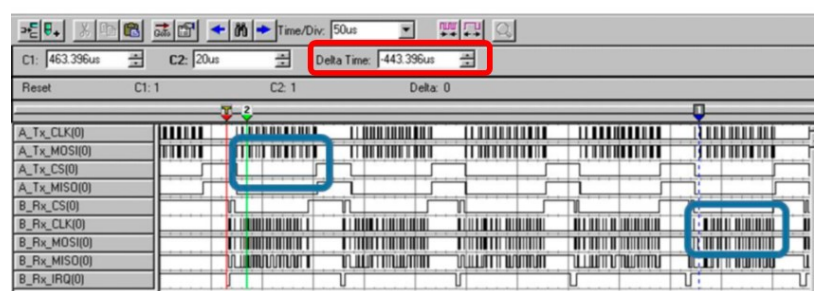


Figure 6. Capture of the transmission and reception between Transmitter and Receiver devices. Blue boxes show correspondent frames in transmission and reception, and the red box highlights the delay between them.

3.4.2. Configuration Frame Transmission

As stated before, the Transmitter device relies on a set of programmable devices that allow to modify the analog input configuration. Each channel can be set in differential or single-ended mode. In the latter case, the reference can also be modified between ground and any of the channels. Additionally, impedance measurement demands controlled

changes in the front-end. Due to ergonomics and utilization convenience, the control panel is located in the Receiver device. This means that the configuration information has to be sent from Receiver to Transmitter, in upstream direction.

It is worth mentioning that during normal utilization of an IOM system, i.e., during a surgical procedure, changes in configuration are scarce and most commonly only carried out at the beginning of the setup of the system. Also, impedance measurement takes place before recording the first signals in order to check that the connections of the electrodes to the patient are good enough. Once the procedure is ongoing, changes are only done if any of the responses monitored is lost or shows a sudden weird behaviour. That being the case, impedance is re-checked to confirm whether the electrodes are well placed or have suffered a disconnection. When this happens, the recording of the signal is interrupted, so a more prolonged transmission delay can be acceptable. These kind of feature is also present in commercial systems, where the impedance measurement procedure interrupts the recording of data.

A state machine implemented in the system we developed manages the communication protocol, as follows. Whenever one of the switches of the control panel is moved, reception state is halted in the Receiver device, and a configuration frame is sent via the transmitting radio towards Transmitter device. This frame comprises a specific header to indicate the type of configuration, and a configuration word, that contains the information required by the Transmitter to vary the corresponding parameters in the analog front-end. The frame is captured by the receiver radio in the Transmitter, issuing an interrupt request to the microcontroller of the device. The recording and transmission of samples is then halted and the system initiates reception state. The microcontroller starts a dialog with the transceiver to extract the received configuration frame out of the FIFO, parsing it and configuring the corresponding programmable switches in the analog front-end. After this, the registering and transmission of samples is resumed, and the whole system returns to normal operation mode.

Assessing a correct configuration is of paramount importance for the reliance on the accuracy of subsequent measurements. Hence, a confirmation protocol is implemented into the dialog between both devices of the system. The flow chart of said protocol is depicted in Figure 7. The starting point is the configuration frame sent by the Receiver (*Config Frame Sent* in Figure 7). In a favourable case, the Transmitter device will receive this frame, and configure the corresponding switches in the analog front-end accordingly to the received information (*Config Dev. A*). The header of the data frame is modified in the subsequent samples, and it will contain a coded value corresponding to the response to the received configuration frame header (*Modify frame Header*). When this configuration is completed (*Successful configuration*), the sampling and sending process is resumed (*Resume sampling*).

After sending the configuration frame, the Receiver falls into a waiting state. If no response is received after a period of time (*Dev. B Reception?*), a timeout is triggered and the configuration frame is re-sent. In case the reception is not successful, the process is repeated several times until a maximum number of trials (M in Figure 7) is reached. If this is the case, the configuration is considered unsuccessful and the user is warned by means of a visual signal in the LEDs (*Incorrect Configuration signal*). On the other hand, if an incoming new data frame is received, its header is extracted and analyzed (*Header correct?*). The configuration is also considered incomplete when the header received by the Receiver is not equal to the one corresponding to the configuration state initially selected and, again, M trials are carried out. If the maximum number of trials is reached ($Error\ counter > M$), the configuration process is considered incorrect and terminated, although it can be started again by activating any of the switches.

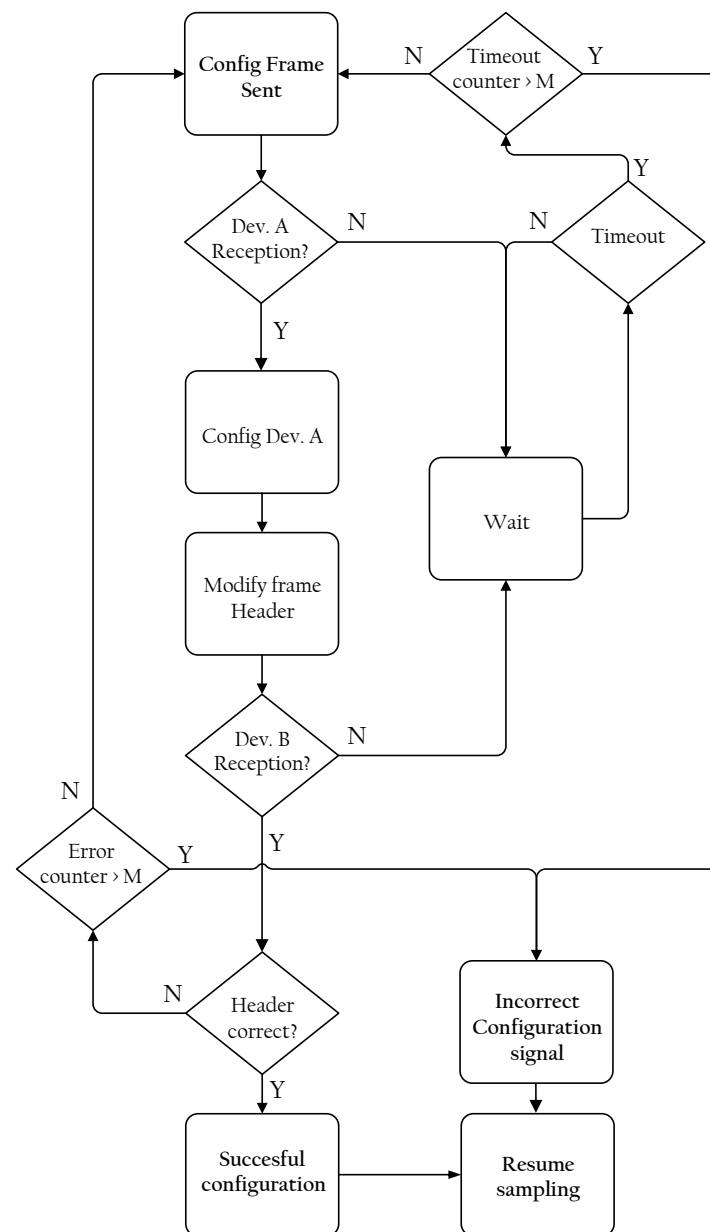


Figure 7. Flowchart of the configuration assessment protocol. Device A is the Transmitter, and Device B is the Receiver. Frame header is utilized to check if the configuration is correct. Two criteria shall be met to obtain a successful configuration: Frame received by Dev. B before a established timeout (*Dev. B Reception?*), and consistent frame header from Dev. A (*Header correct?*). If any of these conditions is not fulfilled, the process is repeated *M* times before considering the configuration incorrect.

The impedance measurement process is also started by a dedicated switch in the control panel of the Receiver device that allows the selection between normal mode or impedance measurement mode. Though automatic, in terms of configuration this technique utilizes the same tools described before, with the only difference that 4 different configurations are needed [16]. If any of these four configurations fails, the measurement is considered unsuccessful and the user will be warned. If the measurement is obtained successfully, the result of the impedance assessment will be shown in the LEDs for each input, indicating a good (green), middling (yellow) or too high (red) contact impedance. The whole algorithm is repeated until the user selects normal operation mode with the

corresponding switch of the control panel. Then, data sampling is resumed and the LEDs go back to their previous state.

4. Results

The prototype was tested in two different setups. Firstly, it was tested in laboratory conditions where recorded signals from real measurements are utilized. Secondly, a set of field tests was carried out, under the same conditions that are expected for the normal operation of the system. Results of the measurements are discussed below.

In both environment, the connectivity has been excellent to very good when transmitter and receiver were located in the same room, or in contiguous rooms like for example the operating room and the preparation/analysis room. Unfortunately, the quality of farther connections depends on too many factors (like type of walls, building geometry, and so on) to be easily quantified. As commented further below, the system has a self-check method to assess if the quality of the connection is acceptable, and will warn the user if not, as well as an algorithm to cope with sample losses. Once the connection is correct, the system proved very robust, with a very low number of lost frames.

4.1. Laboratory Results

Taking into account that the system is composed of several stages both in the Transmitter and the Receiver device, a laboratory setup is arranged in order to assess the correctness and consistency of the signal at all stages of the acquisition and elaboration path.

It is worth noting that the signals commonly recorded by neurophysiological monitoring systems are in the range of micro to millivolts and such low amplitudes are too small for direct monitoring with a standard oscilloscope. In order to tackle this difficulty, the oscilloscope probe is connected at the output of the first stage of amplification, that provides for a gain of at least 50 V/V. This solves the problem of monitoring the input signal, but the same problem arises at the output of the reconstructed waveform at the Receiver side. In this case, we utilized an unused channel of the transmission device as a preamplifier, and the output signal of the Receiver is monitored at the output of the low-noise amplifier of that channel (the configuration is shown using CH2 in Figure 8).

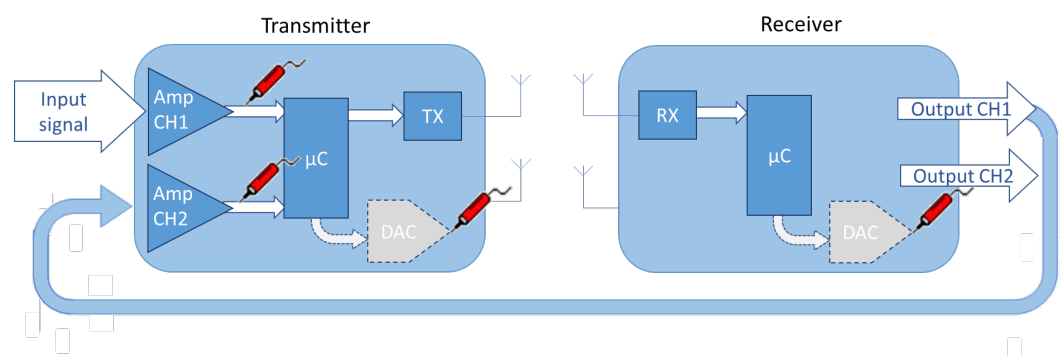


Figure 8. Configuration of the laboratory setup. Given that the noise performances of the first stage amplifier are much better than the oscilloscope's ones, the internal amplifier is used for both the original and the received signal, using different channels in loopback.

Moreover, the microcontroller utilized in both devices of the system includes an integrated DAC, whose output can be wired to the oscilloscope. This allows monitoring also the processes of digitization and sampling, frame construction and transmission. The information corresponding to the channels to be assessed is passed to the internal DAC. Scale factor and different resolutions have to be taken into account, since this internal DAC presents a lower resolution (only 12 bit), in a span of 0 to 3.3 V.

This test arrangement is outlined in Figure 8, where it can be seen that the reconstructed signal, corresponding to the channel 1 input in the Transmitter is wired back to Channel 2 of the same device. A probe symbol indicates where the oscilloscope is connected,

including the output of the first analog amplification stage, as well as the output of the microcontroller-integrated DAC. The rest of the elements of the system have been omitted for the sake of clarity.

Some results of the tests are shown in the oscilloscope captures shown in Figures 9–11. In all the cases, the used input is a response to a MEP that was previously recorded from a volunteer and reproduced by means of a waveform generator. Figure 10 shows a comparison between input analog signal and the result of the digital conversion evaluated through the DAC of the microcontroller. Notice the different scale of the curves. Figure 11 shows a comparison between the analog input signal and the digital signal received and extracted by the Transmitter, again with the help of the internal DAC. Latency between both waveforms is measured with a value close to 800 μ s. Finally, Figure 10 contains a comparison between analog input signal, digital signal in the Receiver, and the output signal, recorded in the output of the first LNA stage in channel 2 of the Transmitter. Because of the duration of the evoked response, latency between original and reconstructed signals is not evident in this case. Nevertheless, correspondence between waveforms can be observed.

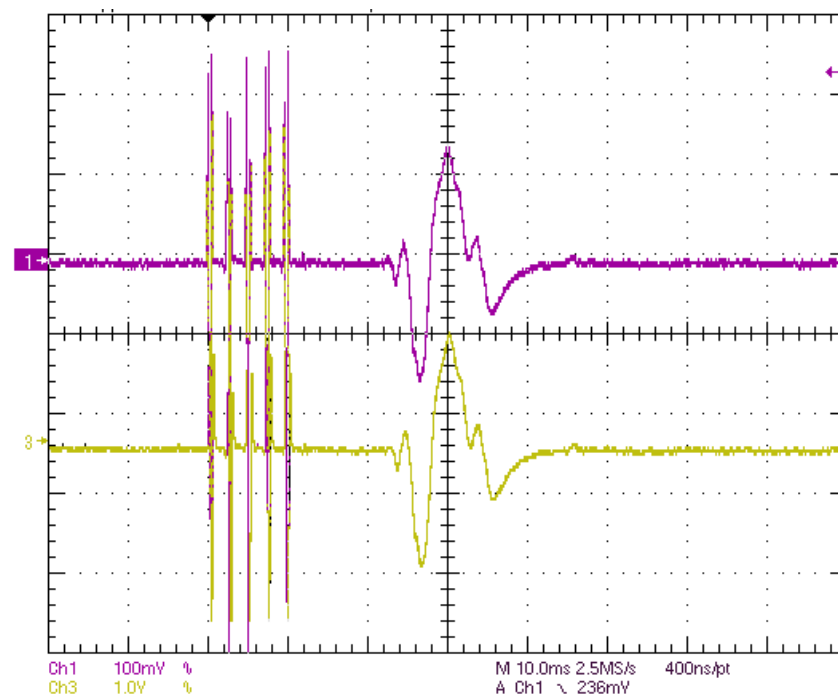


Figure 9. Amplification and ADC stage in Transmitter. Purple track: input signal; Yellowish track: embedded DAC output signal. Horizontal scale is 10 ms/div.

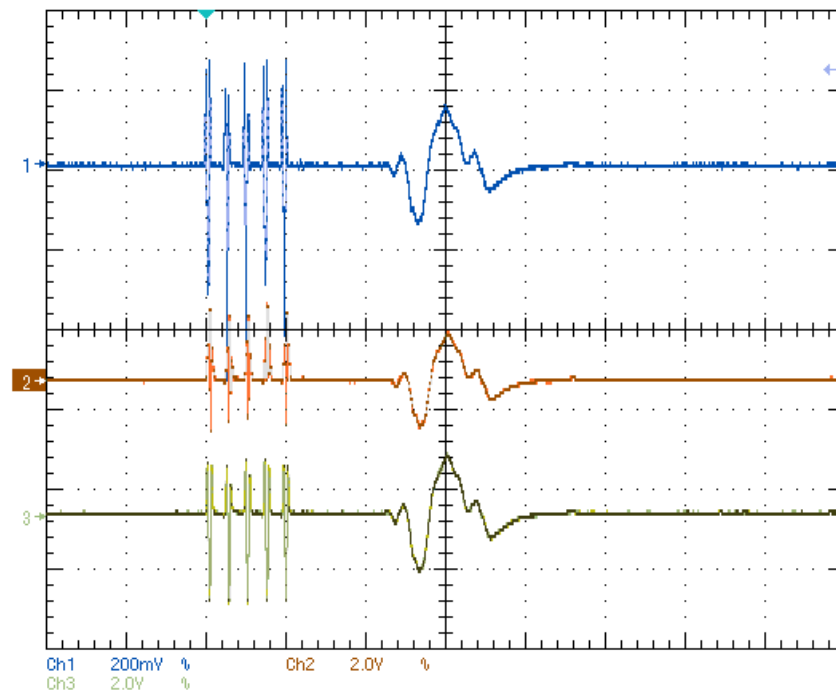


Figure 10. Blue curve: Transmitter input signal; purple curve: Receiver embedded DAC output signal; Olive green track: Receiver analog output signal. Horizontal scale is 10 ms/div.

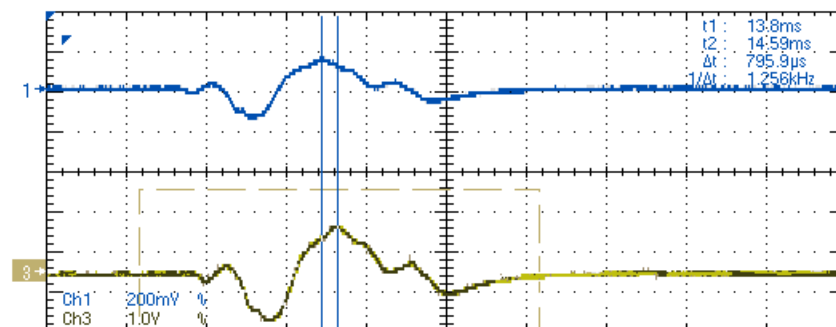


Figure 11. Delay between Transmitter input signal (blue curve), and Receiver embedded DAC output signal (olive green curve). Horizontal scale is 5 ms/div.

4.2. Medical Site Results

In the previous sections, intermediate signals in laboratory tests have been shown in order to check that all the stages of the system work properly. Once this validation phase was completed, several field tests were carried out in order to assess the performance under working conditions with signals coming from a healthy volunteer.

In this case, the experiments take advantage of the utilization of a commercial IONM system that was available in a medical environment. The test setup is sketched in Figure 12. The intraoperative monitoring system that is available is made of three main parts. Firstly, it includes a set of extension adapters with touchproof standard connector inputs, where the electrodes are connected. These adapters are located close to the patient during the surgical procedures. Secondly, the amplifier headbox, where the adapters are connected, is in charge of conditioning and transferring the signals to the visualization section. Lastly, a dedicated PC is connected to the headbox, containing the monitoring software, which is in charge of the plotting and recording of the signals and of the overall configuration. Additionally, the monitoring system has an independent stimulator whose outputs are connected to the patient, but is out of the interest of this test arrangement.

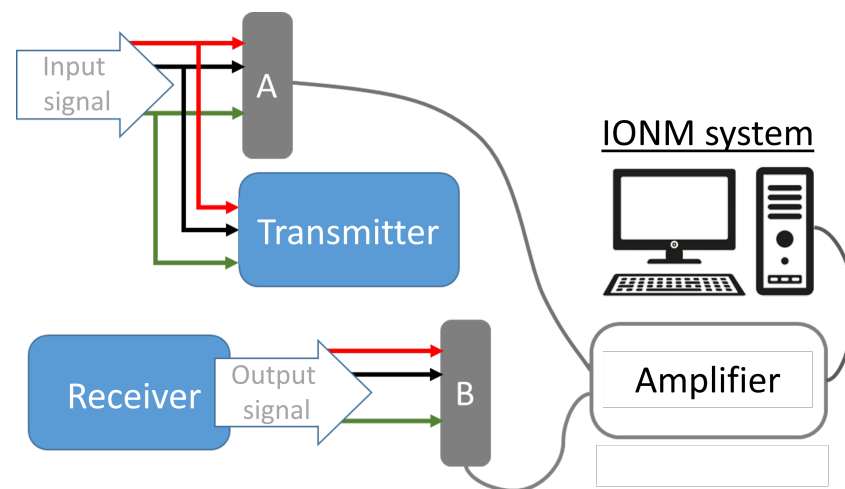


Figure 12. Schematic of the configuration of the performed test.

The input signal coming from the *patient* (in this case, a healthy volunteer) is connected to one of the multichannel input extension adapters of the monitoring system (A). With the help of touch-proof Y connectors, this signal is inserted in parallel in the Transmitter device of the system to be tested. The output of the system, coming out from the Receiver, is then connected to available inputs in a different multichannel adapter (B). Under this arrangement, one can configure the software in order to have a duplicated register of the same biological response, one recorded through A and the other one through B and compare them in the same display window.

Although the system developed is multichannel and allows several signals to be represented at the same time, for the sake of clarity only individual signals are shown in order to carry out the comparison between different signal ranges.

It is important to highlight that the evaluation of this type of signals during a surgery is made visually, with special interest in the changes of each curve registered during the surgery, taking into account the history of the signals and the reference baselines. Latency and changes in amplitude (with respect to the past plots of the same curve) are considered in order to evaluate the neurophysiological status of the patient. This entails that the adequacy of the signal representation can be assessed with a naked-eye comparison, and as so they were evaluated in the medical environment. The figures containing the results are obtained directly as screenshots from the IONM software utilized for the tests.

The first signal shown is Electrocardiography. This monitors the electrical activity of the heart by means of surface electrodes. This is the largest signal tested, with amplitudes of up to 4 mV. The period of the signal is in the range of seconds. Figure 13 shows the result of the measurements taken. The grey curve is the one originally taken from the patient (through A in Figure 12), and the blue curve represents the output of the system under test (through B in Figure 12). A close correspondence between signals can be observed.

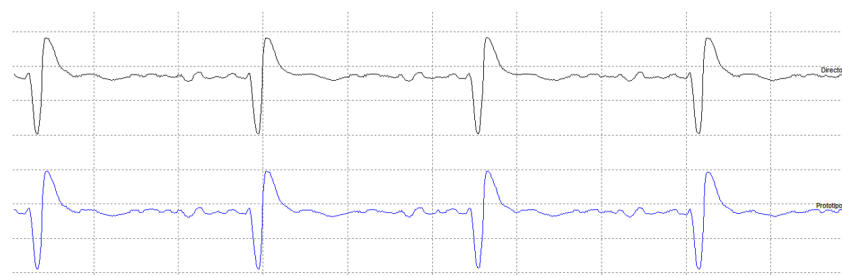


Figure 13. ECG of a healthy volunteer. Grey curve, originally obtained from the system. Blue curve, obtained from the proposed system. Voltage scale is 20 μ V/div, time scale is 300 ms/div.

The next type of signals tested are Motor Evoked Potentials (MEP). These are the response of one or more muscles to a stimulation in motor structures of the brain, typically carried out by scalp electrodes. Figure 14 shows a comparison between two consecutive signals recorded from the test subject directly (left) and through the system developed (right). The timescale is 5 mV/div, and a slight (expected) delay is observed. The small alternate response at the beginning on the curves of the right corresponds to the stimulation artifact. This kind of response is always present in the recorded curves, but the monitoring software usually relies on specific algorithms in order to filter it out or to place just before the origin of the time scale, like in the original pictures on the left. Nevertheless, the representation of this artifact does not pose a problem, since the specialist analyzing the curves will pay attention to the latency between the muscle response and the stimulation, which can be measured easily with the help of screen cursors. Again, a close correspondence between original and reproduced signals is obtained.

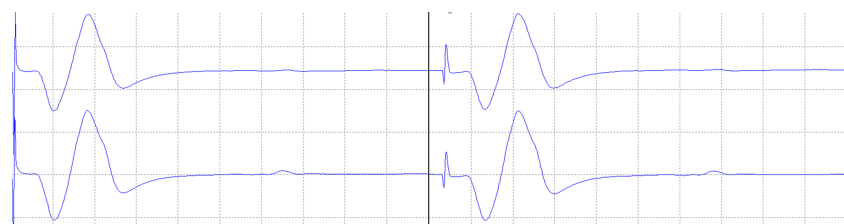


Figure 14. MEP of a healthy volunteer. Curves on the left originally obtained from the system. Curves on the right, obtained from the proposed system. Voltage scale is 2 mV/div, time scale is 5 ms/div.

Another example of the delay of the signal reconstructed is represented in Figure 15, where another pair of MEPs is set against. The blue curve on the top is the original one, and the green curve on the bottom is the reconstructed one. The latter shows a constant delay lower than 2 ms.

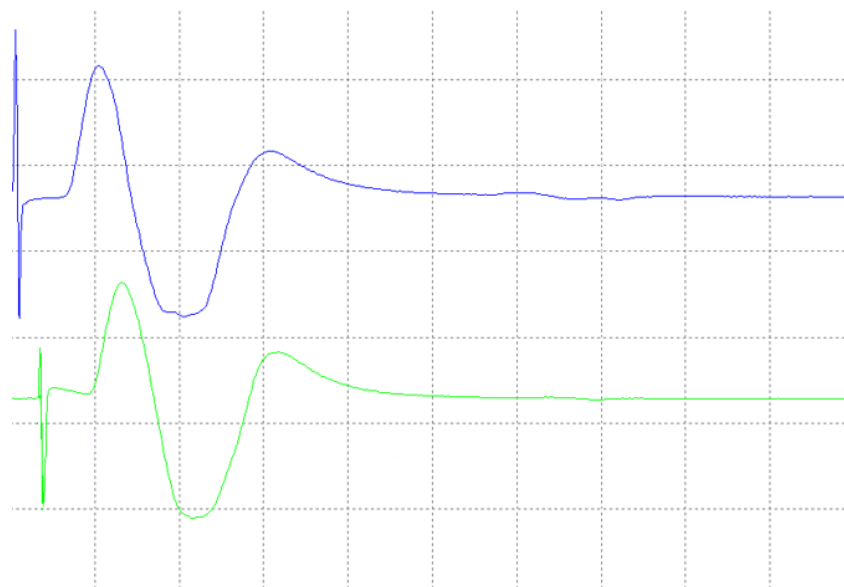


Figure 15. MEP of a healthy volunteer. The blue curve is the one originally obtained from the system. The green curve is obtained with the proposed system. Voltage scale is 5 mV/div, time scale is 5 ms/div.

Because of noise and resolution in analog-to-digital and digital-to-analog conversions, the errors in signal regeneration increase as the amplitude and signal time scale decrease. Because of this, the next type of measurement to be assessed were Somato-Sensory Evoked Potentials (SSEP). These are the record of electrical potentials generated by the somato-sensory pathway in central and peripheral portions of the nervous system, in response

to a stimulus. Typically, stimulation is done in median and tibial nerves (hands and feet), and detection is carried out in the scalp. Because of their small amplitude (in the range of μV), the monitoring software implements special algorithms to average the responses recorded for noise removal, so that the potential can be recognizable after a number of averages, normally between 50 and 150. Figure 16 shows the result of the comparative measurement after 100 averages. Grey and blue curves represent, respectively, the original and reconstructed signals. This case confirms the constant latency in the curve reconstruction, derived for the constant frame rate of the transmission algorithm.

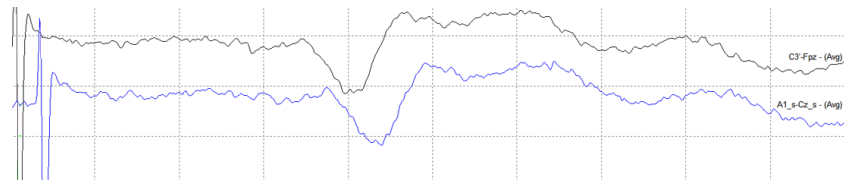


Figure 16. SSEP of a healthy volunteer. Grey curve originally obtained from the system. Blue curve, obtained from the proposed system. Voltage scale is $1 \mu\text{V}/\text{div.}$, time scale is $5 \text{ ms}/\text{div.}$

The measurements shown so far serve as a representative example of different amplification ranges. As described before, the acquisition front-end included in Transmitter device is equipped with a set of programmable gain amplifiers that adapt the amplification range to the voltage level of the signal. This adaptation is made automatically by the algorithm programmed in the microcontroller of the device; notice that the amplitude of the signals shown in Figures 13–16 vary from the millivolt range (MEP and ECG) to the microvolt range (SSEP).

Finally, Auditory Evoked Potential (AEP) signals are tested. These signals are obtained as a response of the auditory system structures to an acoustic stimulus that is produced by means of pads inserted in the patient's inner ear. Correct acquisition and reproduction of these signals is quite challenging in common medical practice and, due to their low amplitudes, the number of required averages is in the range of several hundreds. Besides equivalence between original (grey) and reconstructed (blue) signals, Figure 17 shows a measurement of the constant delay introduced by the system tested. The cursors show a time difference between the peaks of the signal of 1.5 ms . In this case, due to the short time scale of the neural response, the latency caused by acquisition, sampling, transmission, reception and reproduction of the information, the delay is quite pronounced. Given that this can be considered a worst-case scenario, the conclusion is that the delay is still acceptable; the important information here is the presence of the neural response, and the normal window used is, as shown in the diagram, of about 15 ms .

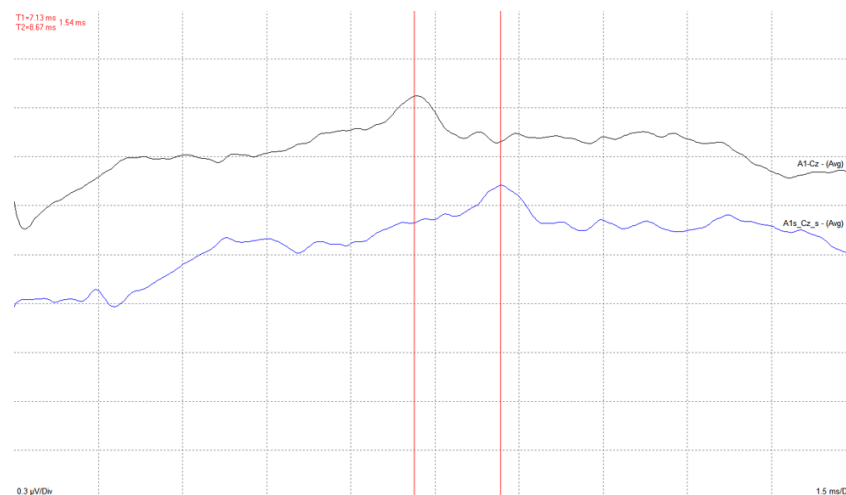


Figure 17. AEP of a healthy volunteer. Grey curve, originally obtained from the system. Blue curve, obtained from the proposed system. Voltage scale is $0.3 \mu\text{V}/\text{div.}$, time scale is $1.5 \text{ ms}/\text{div.}$

5. Discussion

The aim of this article was the discussion of a prototype of a wireless device that can be utilized along with already available intraoperative monitoring devices, that represents, in itself, substantial step toward the definition of a new monitoring paradigm. Tests performed on the prototype that has been designed have demonstrated the ability of the system to satisfactorily address the problems that prompted this investigation. In particular:

- Due to all the stages of the system from signal acquisition to reconstruction, a latency time is introduced. Although this feature is critical in the medical evaluation of the recorded signals, test measurements show that this delay is constant and acceptably low for the intended application.
- Several wireless technologies and protocols were considered, and an ISM RF radio module was selected as the most adequate one. A custom protocol was developed in order to comply with the sampling frequency and low latency requested, including data transmission/reception and configuration commands dialog.
- The system developed is versatile, and input channels can be configured to work as single-ended (referential) or differential inputs. The user has the possibility to change the configuration as well as the channel utilized as the reference for the measurements.
- The system includes a novel impedance measurement method, necessary to assess the correct connection of the electrodes, similarly to what is installed in current commercial monitoring devices. This method is implemented in the analog front end of the system and has been thoroughly described in [16].
- Currently available commercial monitoring systems present a software interface that allows the user to adjust the amplification gain depending on the voltage range of the signal. In our system an algorithm is implemented that analyzes the amplitude of the signal recorded on each channel and automatically changes the setting of the programmable gain amplifiers in the analog front-end.
- The validation of the system has been carried out through laboratory and field tests. The results of the experiments demonstrate sufficient accuracy in signal regeneration across the full range of the expected input signals, as well as an acceptable delay between actual and regenerated signal.

Finally, the market for the IONM devices and systems has been estimated [23] to be around USD 1.6 billions in 2020, and to soar up to about USD 9 billions by 2028; in this scenario the proposed device can fit as a valuable step towards a fully wireless implementation of the monitoring system, offering a cost-effective intermediate solution to the reduction of the cumbersome wiring of the patient to the analysis machines. In addition, the approach of the solution proposed permits the utilization of this technology regardless of the monitoring system used, entailing a substantial advantage in the market.

6. Patents

Part of the described system has been submitted to the European Patent Office as WO 2018/011439 [24] and is in course of evaluation. More in detail, the patent cover the system for analog measurement, transmission and reconstruction of bio-potentials with a fully passive detection of the quality of the electrode-tissue contact. This correspond basically to the structure of Figure 2, the procedure indicated in the flowchart of Figure 7, and the contact impedance assessment procedure described in [16].

Author Contributions: The authors of this Work have been contributing in roughly the same way to the research that lead to this article, and all of them have contributed to writing, proofing and correcting the paper and the associated figures. In detail, E.A.R. contributed all over the map, building the prototype, debugging it, planning the measurements and analyzing them. R.G., G.S. and C.C. were more involved in the analog design; C.R.-M.G., J.M.D. and J.D.M.F. were more involved in the digital design (hardware and software) and PCB optimization; L.V.-Z. and J.P. have supervised and assisted in the field tests. All the authors participated in the debugging of the system, its deployment

and the measurement campaigns, as well as in revising the manuscript. All authors have read and agreed to the published version of the manuscript.

Funding: This research was partially funded by Soinde, S.L.

Institutional Review Board Statement: A series of tests has been performed on human volunteers in the laboratories of the IIT and of the University Hospital “La Princesa”, in Madrid, respecting the internal protocols of the Institute; the experimental protocols were approved by the Ethical Committee of Clinical Research of Hospital de la Princesa (number of register PI-843, approved 21 December 2015).

Informed Consent Statement: The test has been duly authorized, and performed in accordance with the approved protocols, on volunteers whose have been informed and agreed to conduct the experiments, providing specific informed consent, and being fully aware of the risks and methodology of the experiment.

Data Availability Statement: Data is available upon request.

Conflicts of Interest: The authors declare no conflict of interest. Additionally, the funders had no role in the design of the study; in the collection, analyses, or interpretation of data; in the writing of the manuscript; or in the decision to publish the results.

Abbreviations

The following abbreviations are used in this manuscript:

WIONM	Wireless Intraoperative Neurophysiological Monitoring
IONM	Intraoperative Neurophysiological Monitoring
EEG	Electroencephalography
EMG	Electromyography
ECoG	Electrocorticography
ADC	Analog-to-Digital Converter
DAC	Digital-to-Analog Converter
RF	Radio-Frequency
CRC	Cyclic Redundancy Check
SSEP	Somato-Sensory Evoked Potentials
EP	Evoked Potential
MEP	Motor Evoked Potential
AEP	Auditory Evoked Potential

References

- Howick, J.; Cohen, B.A.; McCulloch, P.; Thompson, M.; Skinner, S.A. Foundations for evidence-based intraoperative neurophysiological monitoring. *Clin. Neurophysiol.* **2016**, *127*, 81–90. [\[CrossRef\]](#) [\[PubMed\]](#)
- Vega-Zelaya, L.; Sola, R.G.; Pastor, J. Intraoperative Neurophysiological Monitoring in Neuro-oncology. In *Neurooncology—Newer Developments*; Agrawal, A., Ed.; IntechOpen: Rijeka, Croatia, 2016; Chapter 9.
- Liao, L.D.; Chen, C.Y.; Wang, I.J.; Chen, S.F.; Li, S.Y.; Chen, B.w.; Chang, J.Y.; Lin, C.T. Gaming control using a wearable and wireless EEG-based brain-computer interface device with novel dry foam-based sensors. *J. Neuroeng. Rehabil.* **2012**, *9*, 5. [\[CrossRef\]](#) [\[PubMed\]](#)
- Lin, C.-T.; Ko, L.-W.; Chang, M.-H.; Duann, J.-R.; Chen, J.-Y.; Su, T.-P.; Jung, T.-P. Review of Wireless and Wearable Electroencephalogram Systems and Brain-Computer Interfaces—A Mini-Review. *Gerontology* **2010**, *56*, 112–119. [\[CrossRef\]](#) [\[PubMed\]](#)
- Chi, Y.M.; Cauwenberghs, G. Wireless Non-contact EEG/ECG Electrodes for Body Sensor Networks. In Proceedings of the 2010 International Conference on Body Sensor Networks, Singapore, 7–9 June 2010; pp. 297–301.
- Sodagar, A.M.; Wise, K.D.; Najafi, K. A Wireless Implantable Microsystem for Multichannel Neural Recording. *IEEE Trans. Microw. Theory Tech.* **2009**, *57*, 2565–2573. [\[CrossRef\]](#)
- Vetter, R.J.; Williams, J.C.; Hetke, J.F.; Nunamaker, E.A.; Kipke, D.R. Chronic Neural Recording Using Silicon-Substrate Microelectrode Arrays Implanted in Cerebral Cortex. *IEEE Trans. Biomed. Eng.* **2004**, *51*, 896–904. [\[CrossRef\]](#) [\[PubMed\]](#)
- Casson, A.J.; Yates, D.C.; Smith, S.J.; Duncan, J.S.; Rodriguez-villegas, E. Wearable Electroencephalography. *IEEE Eng. Med. Biol. Mag.* **2010**, *29*, 44–56. [\[CrossRef\]](#) [\[PubMed\]](#)
- Patki, S.; Grundlehner, B.; Verwegen, A.; Mitra, S.; Xu, J.; Matsumoto, A.; Yazicioglu, R.F.; Penders, J. Wireless EEG system with real time impedance monitoring and active electrodes. In Proceedings of the 2012 IEEE Biomedical Circuits and Systems Conference (BioCAS), Hsinchu, Taiwan, 28–30 November 2012; pp. 108–111.

10. Sagha, H.; Perdakis, S.; Chavarriaga, R. Quantifying Electrode Reliability during Brain—Computer Interface Operation. *IEEE Trans. Biomed. Eng.* **2015**, *62*, 858–864. [[CrossRef](#)] [[PubMed](#)]
11. Buxi, D.; Kim, S.; Van Helleputte, N.; Altini, M.; Wijsman, J.; Yazicioglu, R.F.; Penders, J.; Van Hoof, C. Correlation between electrode-tissue impedance and motion artifact in biopotential recordings. *IEEE Sens. J.* **2012**, *12*, 3373–3383. [[CrossRef](#)]
12. Ferree, T.C.; Luu, P.; Russell, G.S.; Tucker, D.M. Scalp electrode impedance, infection risk, and EEG data quality. *Clin. Neurophysiol.* **2001**, *112*, 536–544. [[CrossRef](#)] [[PubMed](#)]
13. Shannon, C. Communication in the Presence of Noise. *Proc. IRE* **1949**, *37*, 10–21. [[CrossRef](#)]
14. Webster, J. *Medical Instrumentation Application and Design*, 4th ed.; John Wiley & Sons: Hoboken, NJ, USA, 2009. Available online: <https://books.google.es/books?id=CQ4cAAAAQBAJ> (accessed on 15 October 2022).
15. AD8429 1nV/ $\sqrt{\text{Hz}}$ Low Noise Instrumentation Amplifier. 2017. Available online: <https://www.analog.com/media/en/technical-documentation/data-sheets/ad8429.pdf> (accessed on 15 October 2022).
16. Alonso, E.; Giannetti, R.; Rodríguez-Morcillo, C.; Matanza, J.; Muñoz-Frías, J.D. A Novel Passive Method for the Assessment of Skin-Electrode Contact Impedance in Intraoperative Neurophysiological Monitoring Systems. *Sci. Rep.* **2020**, *10*, 2819. [[CrossRef](#)] [[PubMed](#)]
17. Scandurra, G.; Cannatà, G.; Giusi, G.; Ciofi, C. A new approach to DC removal in high gain , low noise voltage amplifiers. In Proceedings of the 2017 International Conference on Noise and Fluctuations (ICNF), Vilnius, Lithuania, 20–23 June 2017; pp. 1–4.
18. Huang, C.c.; Hung, S.h.; Chung, J.f.; Van, L.D.; Lin, C.t. Front-End Amplifier of Low-Noise and Tunable BW/Gain for Portable Biomedical Signal Acquisition. In Proceedings of the 2008 IEEE International Symposium on Circuits and Systems (ISCAS), Seattle, WA, USA, 18–21 May 2008; pp. 2717–2720.
19. Harrison, R.R.; Charles, C. A Low-Power Low-Noise CMOS Amplifier for Neural Recording Applications. *IEEE J. Solid-State Circuits* **2003**, *38*, 958–965. [[CrossRef](#)]
20. Müller-Putz, G.R.; Scherer, R.; Neuper, C.; Pfurtscheller, G. Steady-State Somatosensory Evoked Potentials: Suitable Brain Signals for Brain—Computer Interfaces? *IEEE Trans. Neural Syst. Rehabil. Eng.* **2006**, *14*, 30–37. [[CrossRef](#)] [[PubMed](#)]
21. Chestek, C.A.; Gilja, V.; Nuyujukian, P.; Kier, R.J.; Solzbacher, F.; Ryu, S.I.; Harrison, R.R.; Shenoy, K.V. HermesC : Low-Power Wireless Neural Recording System for Freely Moving Primates. *IEEE Trans. Neural Syst. Rehabil. Eng.* **2009**, *17*, 330–338. [[CrossRef](#)] [[PubMed](#)]
22. Farajidavar, A.; Seifert, J.L.; Bell, J.E.S.; Seo, Y.S.; Delgado, M.R.; Sparagana, S.; Romero, M.I.; Chiao, J.C. A wireless system for monitoring transcranial motor evoked potentials. *Ann. Biomed. Eng.* **2011**, *39*, 517–523. [[CrossRef](#)] [[PubMed](#)]
23. IGlobal Intraoperative Neuromonitoring (IONM) Market to Reach USD 9.03 Billion by 2028: Vantage Market Research. 2021. Available online: <https://www.globenewswire.com/en/news-release/2021/11/18/2337755/0/en/Global-Intraoperative-Neuromonitoring-IONM-Market-to-Reach-USD-9-03-Billion-by-2028-Vantage-Market-Research.html> (accessed on 15 October 2022).
24. Jiménez-Carles Gil-Delgado, E. Intraoperative Monitoring System. Patent Application WO 2018/011439 A1, 18 January 2018. Available online: <https://patentscope.wipo.int/search/es/detail.jsf?docId=WO2018011439> (accessed on 15 October 2022).